0026-895X/05/6704-1034–1044$20.00
MOLECULAR PHARMACOLOGY
Copyright © 2005 The American Society for Pharmacology and Experimental Therapeutics
Mol Pharmacol 67:1034–1044, 2005

Vol. 67, No. 4
7187/1196869
Printed in U.S.A.

Anuroctoxin, a New Scorpion Toxin of the α-KTx 6 Subfamily, Is Highly Selective for Kv1.3 over IKCa1 Ion Channels of Human T Lymphocytes[S]

Miklós Bagdány, Cesar V. F. Batista, Norma A. Valdez-Cruz, Sándor Somodi, Ricardo C. Rodriguez de la Vega, Alexei F. Licea, Zoltán Varga, Rezső Gáspár, Lourival D. Possani, and György Panyi

Department of Biophysics and Cell Biology, University of Debrecen, Medical and Health Science Center, Debrecen, Hungary (M.B., S.S., Z.V., R.G., G.P); Department of Molecular Medicine and Bioprocesses, Institute of Biotechnology, National Autonomous University of Mexico, Avenida Universidad, Cuernavaca, Mexico (C.V.F.B., N.A.V.-C., R.C.R.-V., L.D.P.); and Laboratory of Molecular Immunology and Biotoxins, Centro de Investigación Científica y de Educación de Ensenada, Ensenada, Mexico (A.F.L.)

Received September 15, 2004; accepted December 21, 2004

ABSTRACT

The physiological function of T lymphocytes can be modulated selectively by peptide toxins acting on Kv1.3 K^+ channels. Because Kv1.3-specific peptide toxins are considered to have a significant therapeutic potential in the treatment of autoimmune diseases, the discovery of new toxins is highly motivated. Through chromatographic procedures and electrophysiological assays, using patch-clamp methodology, the isolation of a novel peptide named anuroctoxin was accomplished using the venom of the Mexican scorpion *Anuroctonus phaiodactylus*. It has 35 amino acid residues with a molecular weight of 4082.8, tightly bound by four disulfide bridges whose complete covalent structure was determined. It has a pyroglutamic acid at the N-terminal region and an amidated C-terminal residue. Sequence comparison and phylogenetic clustering analysis classifies anuroctoxin into subfamily 6 of the α-KTx scorpion toxins (systematic name, α-KTx 6.12). Patch-clamp experiments show that anuroctoxin is a high-affinity blocker of Kv1.3 channels of human T lymphocytes with a K_d of 0.73 nM, and it does not block the Ca^{2+}-activated IKCa1 K^+ channels. These two channels play different but important roles in T-lymphocyte activation. Furthermore, the toxin practically does not inhibit *Shaker* IR, mKv1.1, and rKv2.1 channels, whereas the affinity of anuroctoxin for hKv1.2 is almost an order of magnitude smaller than for Kv1.3. The pharmacological profile and the selectivity of this new toxin for Kv1.3 over IKCa1 may provide an important tool for the modulation of the immune system, especially in cases in which selective inhibition of Kv1.3 is required.

Two types of ion channels dominate the K^+ conductance in human T cells: the voltage-gated Kv1.3 channel belonging to the *Shaker* family of channels (Matteson and Deutsch, 1984), and the Ca^+-activated IKCa1 channel (also known as $K_{Ca}3.1$) (Grissmer et al., 1993). One major physiological function of these channels is the maintenance of a negative membrane potential, which facilitates sustained Ca^{2+} signaling during T-cell activation by providing the electrical driving force for Ca^{2+} entry through voltage-independent Ca^{2+} channels. Peptide and small-molecule inhibitors of the channels depolarize the membrane, resulting in the inhibition of Ca^{2+} signaling and lymphocyte proliferation (Chandy et al., 2004; Panyi et al., 2004).

All quiescent human T lymphocytes express dominantly Kv1.3 channels (~300 per cell) and a small number of IKCa1

Supported in part by grants 40251Q from the National Council of Science and Technology (Mexican Government) and IN206003 from Dirección General de Asuntos del Personal Académico UNAM (to L.D.P.). Support from grants OTKA TS040773, ETT 222/2003, OTKA T043087, T048740, F035251 (to R.G. and G.P.), and bilateral collaboration program CONACyT-Mexico and TéT-Hungary are highly appreciated. Z.V. and G.P. were supported by the Békésy Fellowship.

Laboratories in the Department of Biophysics and Cell Biology, University of Debrecen and Department of Molecular Medicine and Bioprocesses, Institute of Biotechnology, Cuernavaca, contributed equally to the work.

This work was presented previously in abstract form (*Biophys J* **86:**538A, 2004).

[S] The online version of this article (available at http://molpharm.aspetjournals.org) contains supplemental material.

Article, publication date, and citation information can be found at http://molpharm.aspetjournals.org.

doi:10.1124/mol.104.007187.

ABBREVIATIONS: T_{CM}, central memory T cell; T_{EM}, effector memory T cell; MS/MS, tandem mass spectrometry; LC/MS, liquid chromatography/mass spectrometry; ShK, *Stichodactyla helianthus* peptide; *Shaker* IR, N-terminal inactivation domain-deleted *Shaker* K^+ channel; KTx, K^+-channel–specific scorpion toxin; ChTx, charybdotoxin; MgTx, margatoxin; MauTx, maurotoxin; Ntx, noxiustoxin; HPLC, high-performance liquid chromatography; Arg-C, arginine-C; Cll-dlp, defensin-like peptide isolated from the hemolymph of the scorpion *Centruroides limpidus limpidus*; MSA, multiple sequence alignment; GFP, green fluorescence protein; RF, remaining fraction of the current.

channels (~8–10/cell) (Cahalan et al., 2001; Panyi et al., 2004). Depending on the nature and physiological function of the T cells [i.e., naive, central memory (T_{CM}) and effector memory (T_{EM}) T cells (Sallusto et al., 2004)], their activation induces a specific change in the K^+-channel repertoire (Wulff et al., 2003). Naive and T_{CM} cells acquire an $IKCa1^{high}Kv1.3^{low}$ channel phenotype upon activation (~500 IKCa1 and Kv1.3 channels/cell). In contrast, activation of effector memory T cells (T_{EM}) is accompanied by an increase in the number of Kv1.3 channels to ~1500/cell without any change in the IKCa1 levels; thereby the channel phenotype of the activated T_{EM} becomes $IKCa1^{low}Kv1.3^{high}$ (Wulff et al., 2003).

The difference in the K^+-channel dominance in these T-cell subsets allows specific interference with their activation using selective blockers of Kv1.3 or IKCa1 channels (Chandy et al., 2004). Proliferation of encephalogenic T_{EM} cells, which play a significant role in the pathogenesis of multiple sclerosis, can be suppressed by selective Kv1.3 inhibitors, whereas naive and T_{CM} T cells escape Kv1.3 block-mediated inhibition of proliferation by up-regulating IKCa1 (Wulff et al., 2003). This selective immunosuppression places the isolation of selective Kv1.3 inhibitors into the focus of ongoing research in several laboratories because these molecules are considered to have significant therapeutic potential (Chandy et al., 2004; Panyi et al., 2004).

Scorpion venoms contain peptides that block or modulate the activity of ion channels of excitable and nonexcitable cells (Miller, 1995; Garcia et al., 2001; Chandy et al., 2004; Rodriguez de la Vega and Possani, 2004). The K^+-channel–specific scorpion toxins (KTx) were earlier classified into three (α, β, and γ) distinct families (Tytgat et al., 1999). The α-KTx family of peptides is the best studied thus far, from which 19 subfamilies have been described previously (Rodriguez de la Vega and Possani, 2004; Xu et al., 2004). These toxins were invaluable tools in the identification of specific cellular functions mediated by ion channels and were used as molecular calipers to map the pore architecture of K^+ channels before the three-dimensional X-ray crystallographic structure of these channels was known (Miller, 1995; Garcia et al., 2001; Pardo-Lopez et al., 2002; Jiang et al., 2003).

Several natural peptide blockers of Kv1.3 channels were isolated from scorpions having very high affinity for Kv1.3. The most potent ones, charybdotoxin (ChTx), margatoxin (MgTx), and Pi2 toxin from *Pandinus imperator*, are characterized by equilibrium dissociation constants in the low nanomolar and picomolar ranges (Chandy et al., 2004). Some of these toxins, such as MgTx, display natural selectivity for Kv1.3 over IKCa1 (Leonard et al., 1992). The specificity of Kv1.3 inhibition was increased in the case of ShK toxin, a very high-affinity blocker of Kv1.3 isolated from the sea anemone *Stichodactyla helianthus*, by introducing a non-natural amino acid in position 22 of the peptide ($ShK\text{-}Dap^{22}$) (Kalman et al., 1998). The diversity of the primary sequence of these peptide inhibitors and their valuable pharmacological effects stimulate the search for new molecules in the venoms of different scorpions that were shown to be extremely rich sources of these peptides (Rodriguez de la Vega and Possani, 2004).

In this report, we describe the isolation and functional characterization of a novel peptide toxin, anuroctoxin, from the venom of the scorpion *Anuroctonus phaiodactylus* belonging to the Iuridae family. This is the first report to characterize an active peptide in the venom of this scorpion. The most interesting finding, besides the unique primary structure of anuroctoxin (systematic number, α-KTx 6.12), is that it blocks Kv1.3 channels of human T lymphocytes with high affinity but does not affect calcium-activated IKCa1 channels in the same cells.

Materials and Methods

Source of Venom and Chemicals. Scorpions from the species *A. phaiodactylus* were collected on the hills of Maneadero, Baja California, Mexico, and were electrically stimulated for venom, as described earlier (Valdez-Cruz et al., 2004). All chemicals used in this work were analytical grade reagents as indicated in our earlier publications (Batista et al., 2004; Valdez-Cruz et al., 2004). The chemicals used for the electrophysiological experiments were as described earlier (Peter et al., 2001). High-quality water (bidistilled over quartz) was used for all of the solutions.

Isolation Procedure. The soluble venom was separated by high-performance liquid chromatography (HPLC) using an analytical C18 reverse column from Vydac (Hisperia, CA) in conditions similar to those described previously (Valdez-Cruz et al., 2004). In short, a linear gradient from solution A [0.12% (v/v) trifluoroacetic acid in water] to 60% solution B [0.10% (v/v) trifluoroacetic acid in acetonitrile] run for 60 min was able to resolve many different fractions and/or components. The most active fraction as determined in our electrophysiological system (see below) was further purified using a distinct gradient from solution A to 30% solution B run for 60 min in the same system. The purity of the peptide was ascertained by a symmetrical peak on the HPLC system, amino acid sequencing, and mass spectrometry analysis.

Amino Acid Sequence and Mass Spectrometry Analysis. Automatic amino acid sequencing determination, by Edman degradation, was performed using a Beckman LF 3000 Protein Sequencer (Beckman Coulter, Inc., Fullerton, CA) with the native peptide and its fragments generated by enzymatic cleavage with endopeptidases lysine-C and arginine-C (Arg-C), both from Boehringer Ingelheim GmbH (Ingelheim, Germany), in the same conditions described for another component of the same venom (Valdez-Cruz et al., 2004). Mass spectrometry analysis was performed using a Finnigan LCQ^{Duo} ion trap mass spectrometer (Thermo Finnigan, San Jose, CA) as also described elsewhere (Batista et al., 2004; Valdez-Cruz et al., 2004).

Disulfide Bridge Determination. The disulfide bridge arrangement of the toxin was obtained by cleaving the native peptide with trypsin (Promega, Madison, WI) and chymotrypsin (Boehringer Ingelheim GmbH) in the presence of 150 mM Tris-HCl buffer, pH 6.8, overnight at 37°C, but without reduction and alkylation of the sample in such a way to conserve the disulfide pairing intact. Under liquid chromatography/mass spectrometer (LC/MS) separation, the resulting peptides were fragmented by MS/MS in the same manner as described previously by our group (Batista et al., 2004; Valdez-Cruz et al., 2004).

Sequence Analysis and Phylogenetic Studies. The amino acid sequence of anuroctoxin was analyzed by BLAST and FASTA searches. Both retrieved only α-KTx peptides, although with low similarity scores. To perform a more in-depth analysis, the full set of α-KTx currently available in the literature plus a putative paralogous protein, a defensin-like peptide isolated from the hemolymph of the scorpion *Centruroides limpidus limpidus* (abbreviated Cll-dlp) (Rodriguez de la Vega et al., 2004), was used to generate a multiple sequence alignment (MSA) with MUSCLE (Edgar, 2004). The MSA was then slightly refined to avoid obvious structural inconsistencies. Next, the MSA was used to perform a Bayesian estimation of tree topology using MrBayes 3.0 (Ronquist and Huelsenbeck, 2003) with the amino acid substitution model used by Jones et al. (1992). One-half million Markov chain Monte Carlo iterations were performed,

allowing the program to sample between one cold and two heated chains. The phylogenetic trees were sampled every 250th generation, and the resulting sets were used to calculate a consensus tree with a 50% majority rule. The convergence was achieved around the 200,000th generation. For this reason, the first 1000 samples (corresponding to 250,000 generations) were discarded for the final consensus tree calculation. During the analysis, all the trees were rooted with Cll-dlp.

Homology Modeling. The starting model was generated on Swiss-Modeler (Schwede et al., 2003; http://swissmodel.expasy.org) suite with the structure of HsTx1 as template [Protein Data Bank (PDB) code 1quz]. A user-defined alignment was necessary because anuroctoxin has one residue less than HsTx1 within the core of the molecule. This model was minimized with the NAMD 2.5 (Kale et al., 1999) program until a gradient tolerance of 10^{-9} was achieved, and then a molecular dynamics simulation of 2 ns (900,000 steps, 310 K) was performed to assess stability of the model. Minimization and molecular dynamics were performed within a square cage of 930 water molecules. Stereochemical quality of both starting and final models was assessed by WAT_CHECK (http://www.cmbi.kun.nl/gv/whatcheck).

Cell Preparation. Lymphocyte separation. Kv1.3 and IKCa1 currents were measured in human peripheral T lymphocytes. Heparinized human peripheral venous blood was obtained from healthy volunteers. Mononuclear cells were separated by Ficoll-Hypaque density gradient centrifugation. Collected cells were washed twice with Ca^{2+}- and Mg^{2+}-free Hanks' solution containing 25 mM HEPES buffer, pH 7.4. Cells were cultured in a 5% CO_2 incubator at 37°C in 24-well culture plates in RPMI 1640 medium supplemented with 10% fetal calf serum (Hyclone Laboratories, Logan, UT), 100 μg/ml penicillin, 100 μg/ml streptomycin, and 2 mM L-glutamine at 0.5×10^6/ml density for 3 to 4 days. The culture medium also contained 2.5 or 5 μg/ml phytohemagglutinin A (Sigma-Aldrich Kft, Budapest, Hungary) to increase K^+-channel expression (Deutsch et al., 1986). T lymphocytes were selected for current recording by incubation with mouse anti-human CD2 (BD Biosciences, San Jose, CA) followed by selective adhesion to Petri dishes coated with goat anti-mouse IgG antibodies (Biosource International, Camarillo, CA), as described by Matteson and Deutsch (1984). Dishes were washed gently five times with 1 ml of normal extracellular bath medium (see below) for the patch-clamp experiments.

Cytotoxic murine T cells (CTLL-2) were transiently cotransfected with plasmids for CD4 and for rat Kv2.1 (rKv2.1, a kind gift from Dr. S. Korn, University of Connecticut, Storrs, CT) or *Shaker* IR channels (a kind gift form Dr. G. Yellen, Harvard Medical School, Boston, MA) at a molar ratio of 1:5 or 1:8 (32 or 48 μg/ml total DNA) using electroporation (Deutsch and Chen, 1993). CTLL-2 cells were cultured in RPMI 1640 medium supplemented with 10% fetal bovine serum (Hyclone), 2 mM sodium pyruvate, 10 mM HEPES, 4 mM L-glutamine, 50 μM 2-mercaptoethanol, and 100 CU/ml interleukin-2. Before transfection, cells were cultured for 24 h in fresh medium and collected in the logarithmic phase of growth. After harvesting, cells were suspended in Hanks' 20 mM HEPES balanced salt solution, pH 7.23, at 2×10^7 cells/ml, and the appropriate mixture of DNA was added to the cell suspension. This suspension was transferred to electroporation cuvettes (400 μl/cuvette, 4 mm electrode gap), kept on ice for 10 min, and then electroporated using a BTX electroporator (BTX, San Diego, CA) with the following settings: 725 V/cm, 2350 μF, and 13 Ω. The resultant time constants were 24 to 25 ms. Cells were incubated for an additional 10 min on ice and then transferred back to the culture medium ($\sim 0.5 \times 10^6$ cells/ml) supplemented with 5 mM sodium butyrate (at 37°C, 5% CO_2). Cells were used for electrophysiology between 8 to 16 h after the transfection. The selection of transfectants for electrophysiological recordings was performed using a selective monoclonal adhesion strategy, as described above, but using monoclonal mouse anti-human CD4 antibody (0.5 mg/10^6 cells).

Cos-7 cells were transiently cotransfected with plasmids for green fluorescence protein (GFP) and for hKv1.2 (pcDNA3/Hygro vector containing the full coding sequence for Kv1.2, a kind gift from Dr. S. Grissmer, University of Ulm, Ulm, Germany) at a molar ratio of 1:5 using LipofectAMINE 2000 reagent according to the manufacturer's protocol (Invitrogen, Carlsbad, CA) and cultured under standard conditions. Currents were recorded 2 to 3 days after transfection. GFP-positive transfectants were identified in a Nikon TE2000U fluorescence microscope (Nikon, Tokyo, Japan. More than 70% of the GFP-positive cells expressed Kv1.2 currents.

L929 and B82 cells stably expressing mKv1.1 and rKv1.2 channels have been described earlier (Grissmer et al., 1994) and were kind gifts from Dr. Heike Wulff (University of California, Davis, Davis, CA).

Electrophysiology. Whole-cell currents were measured in voltage-clamped cells using an Axopatch 200A amplifier connected to a personal computer using Axon Digidata 1200 data acquisition hardware (Axon Instruments Inc., Union City, CA). Series resistance compensation up to 85% was used to minimize voltage errors and achieve good voltage-clamp conditions. Pipettes were pulled from GC 150 F-15 borosilicate glass capillaries in five stages and fire-polished, resulting in electrodes having 2- to 3-MΩ resistance in the bath. The bath solution consisted of 145 mM NaCl, 5 mM KCl, 1 mM $MgCl_2$, 2.5 mM $CaCl_2$, 5.5 mM glucose, and 10 mM HEPES, pH 7.35, supplemented with 0.1 mg/ml bovine serum albumin (Sigma-Aldrich). The measured osmolarity of the external solution was between 302 and 308 mOsm. The internal solution consisted of 140 mM KF, 2 mM $MgCl_2$, 1 mM $CaCl_2$, 10 mM HEPES, and 11 mM EGTA, pH 7.22 except for calcium-activated potassium current measurement, when 150 mM potassium aspartate, 5 mM HEPES, 10 mM EGTA, 8.7 mM $CaCl_2$, and 2 mM $MgCl_2$, pH 7.2, was used. In the latter case, the concentration of free Ca^{2+} was 1 μM in the pipette solution. The measured osmolarity of the internal solutions was approximately 295 mOsm. Bath perfusion around the measured cell with different test solutions was achieved using a gravity-flow perfusion setup with eight input lines and polyethylene tube output tip with flanged aperture to reduce the turbulence of the flow. Different extracellular solutions were exchanged in the recording chamber by a gravity-driven, computer-controlled system. Excess fluid was removed continuously. For data acquisition and analysis, the pClamp8 software package (Axon Instruments) was used. Before analysis, whole-cell current traces were corrected for ohmic leak and digitally filtered (three-point boxcar smoothing).

Results

Isolation and Structural Characterization of Anuroctoxin. The soluble venom of *A. phaiodactylus* is separated to at least 70 different components by HPLC (see *Materials and Methods*), as shown in Fig. 1A. The fraction eluting at 20.42 min blocked Kv1.3 currents of human T lymphocytes with high affinity (data not shown) and was further purified as shown in the inset of Fig. 1A. Some of the remaining fractions and/or components when assayed blocked the Kv1.3 currents at a much higher concentration, at least 2 orders of magnitude higher, and were considered not effective (data not shown). The inset graphic result shows the elution of a major component (the peptide under study) plus some minor contaminants that are discarded. This peptide applied to the amino acid sequencer gave no sequence, suggesting that it was blocked at the N-terminal region, but under mass spectrometry analysis showed the presence of a single component with a molecular weight of 4082.8. Three main peptides were obtained after enzymatic hydrolysis with Arg-C endopeptidase, as indicated by the continuous line, under the sequence shown in Fig. 1B. The most N-terminal–situated one, when sequenced, gave no results (it was

blocked), suggesting that it was the N-terminal peptide, but when cleaved with lysine-C endopeptidase, it allowed the determination of the amino acid sequence from residues in position Glu3 to Lys18 by two independent methods: automatic Edman degradation (underlined with a dotted line), and MS/MS fragmentation (underlined with a broken line). The entire sequence of this peptide was also confirmed by MS/MS analysis (underlined with a solid line). The subpeptide corresponding to the positions Asn17 to Lys28 was sequenced and correctly aligned after mass fragmentation (MS/MS) of several peptides obtained by enzymatic hydrolysis as indicated under the sequence of Fig. 1B. The last segment was sequenced and positioned correctly into the sequence as derived from the results of overlapping sequences obtained by mass fragmentation, as indicated. The fact that the peptide from position Cys29 to Lys35 had an amidated lysine at the end (last amino acid) indicates the position of this subpeptide in the sequence.

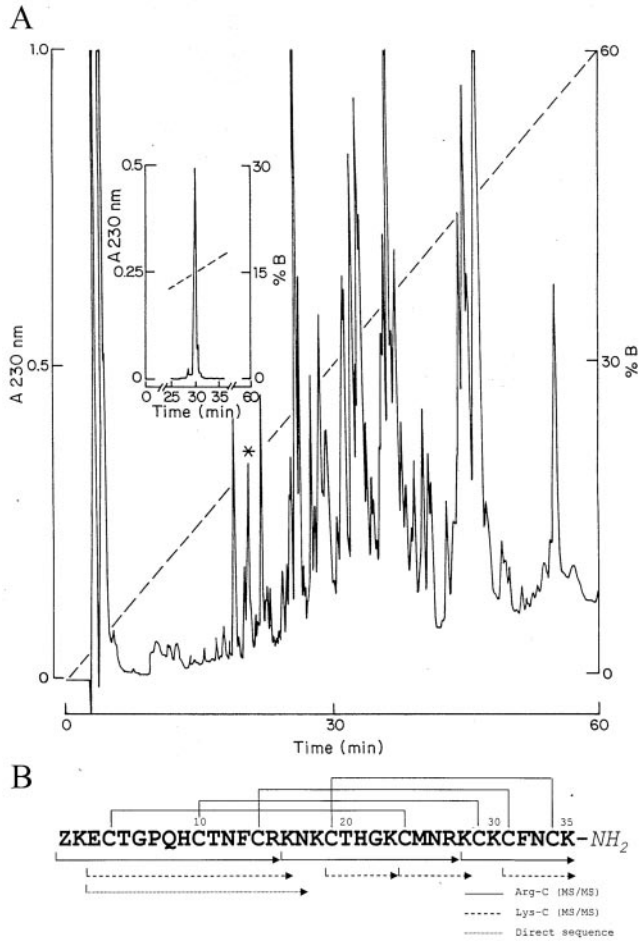

Fig. 1. Purification and covalent structure of anuroctoxin. A, 1 mg of soluble venom from *A. phaiodactylus* was separated by HPLC using a C18 reverse-phase column, eluted with a linear gradient from solution A to 60% solution B run for 60 min. The fraction labeled with the asterisk was rechromatographed in the same system and run from solution A to 30% solution B in 60 min. The major component is pure anuroctoxin and corresponds to approximately 1.1% of the total soluble venom. B, the complete amino acid sequence of anuroctoxin was obtained by a combination of direct Edman degradation and mass spectrometry fragmentation of several peptides obtained by enzymatic hydrolysis of anuroctoxin, as indicated by the segments underlined by solid, dotted, and broken lines. Solid lines linking the cysteine residues indicate the disulfide bridges in positions Cys4 to Cys24, Cys10 to Cys29, Cys14 to Cys31, and Cys19 to Cys34. The N-terminal pyroglutamic acid and the C-terminal amidated lysine were determined by mass spectrometry (MS/MS) fragmentation.

Additional confirmation of the sequence came from the results aimed at the determination of the disulfide bridges, from which representative results are shown in Fig. 2. For this purpose, the native toxin was digested with trypsin and chymotrypsin in a slightly acidic buffer (see *Materials and Methods*) without prior reduction of the sample in such a way as to leave the disulfide pairing intact. This procedure, followed by LC/MS on line and tandem fragmentation (MS/MS), allowed for the identification of two disulfide bridges: one between Cys4 and Cys24 and the other between Cys10 and Cys29 (Fig. 2, A and B). As it can be seen in these mass spectra, the N-terminal amino acid is compatible with the presence of a pyroglutamic acid at this position, confirming that the native peptide is blocked at the most N-terminal–situated residue. The third disulfide pairing formed by Cys14 to Cys31 was obtained by mass fragmentation (MS/MS) of the heterodimeric peptide with a molecular weight of 544.5 (theoretical value) and 544.5 (found), which corresponds to the sequence Cys14 to Arg15 and Cys31 to Phe32 of the sequence (data not shown). The amidation of Lys35 is clearly shown in Fig. 2C. The theoretical molecular weight expected was 973.3, but the weight experimentally determined was 972.3, suggesting that the last residue was amidated. This was later confirmed by MS/MS fragmentation (Fig. 2C). The completeness of the full sequence was also verified by the addition of the molecular masses found for each one of the three separated peptides after the first enzymatic cleavage with Arg-C endopeptidase. The theoretical expected and the experimentally found molecular weights are the same (4082.8). In addition, the disulfide pairing is made between cysteines that occupy the same relative position in other α-KTx scorpion toxins. Thus, the folding of the disulfide bridges for anuroctoxin is equivalent to the other scorpion toxins that recognize K^+ channels.

Phylogenetic Clustering Analysis. When the amino acid sequence of anuroctoxin was compared against all the known α-KTxs (81 to date), the identities fall lower than 50% against any of the toxins considered (Fig. 3). This low-sequence relatedness is similar to the one that segregates α-KTx subfamilies 1 and 16 or between members of more divergent subfamilies (e.g., α-KTx 6). In the present case, to determine whether anuroctoxin belongs to 1 of the 19 previously assigned α-KTx subfamilies, a phylogenetic analysis was performed comprising all of the peptides belonging to the α-KTx family. First, the sequences were aligned using MUSCLE (Edgar, 2004) and refined manually for structural inconsistencies, and then a Bayesian estimation of the tree topology was performed using MrBayes 3.0 (Ronquist and Huelsenbeck, 2003). MrBayes uses Bayesian inference and Markov chain Monte Carlo sampling scheme to calculate posterior probability of a given tree topology. According to this analysis, anuroctoxin falls in a strongly supported cluster, including two sisters of α-KTx subfamilies, namely, 6 and 7. It is rather closely branched to subfamily 6; thus, we propose the systematic number α-KTx 6.12 for anuroctoxin. A representative Bayesian-inferred tree is shown in Fig. 4. Numbers under internal nodes highlight strongly supported clusters; they represent Bayesian posterior probability ($\times$100) of finding a given partition during the tree-sampling procedure.

Block of Kv1.3 Channels by Anuroctoxin. Fig. 5 shows the effects of anuroctoxin on Kv1.3 currents measured in whole-cell voltage-clamped human peripheral blood T lymphocytes. Under the experimental conditions applied (detailed under *Materials and Methods* and in the legend to Fig. 5), the whole-cell currents were conducted exclusively by Kv1.3 channels (Peter et al., 2001). On the basis of 10 pS single-channel conductance, the number of Kv1.3 channels per T cell was between 1000 and 2000. Fig. 5A displays macroscopic K^+ currents through Kv1.3 channels recorded sequentially in the same cell, before (control) and after the addition of 0.5 nM anuroctoxin to the external solution. The displayed record in the presence of anuroctoxin was taken after the equilibration of the block. Under these conditions, approximately 50% of the channels were blocked. The block was completely reversed by perfusing the cell with toxin-free external solution (washout, record shown after full recovery from block).

The reversibility of the K^+ current block by 0.5 nM anuroctoxin is also clearly demonstrated in Fig. 5, B and C. The

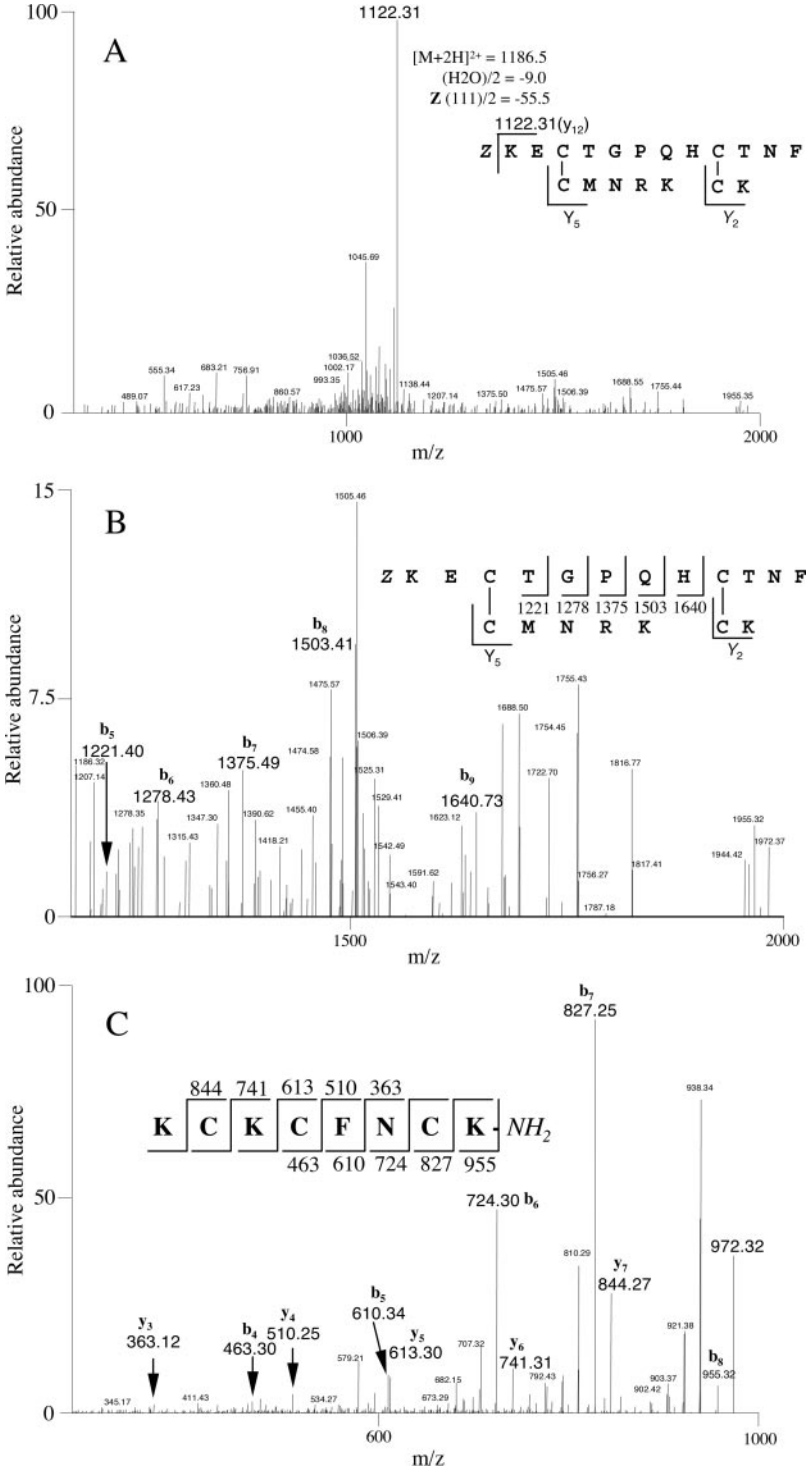

Fig. 2. Mass spectrometry analysis of anuroctoxin peptides. A, tandem mass spectrum of the precursor ion at mass/charge (*m/z*) 1186.5 ($[M + 2H]^{2+}$) generated by trypsin and chymotrypsin digestion after analysis by LC/MS, showing the dominant fragment Y5*Y*2y12 with a molecular weight of 1122.31, which corresponds to the loss of pyroglutamic acid at the N-terminal segment. B, magnification of the collision-induced dissociation spectrum shown in A, from *m/z* range 1160 to 2000 of the parent ion $[M + 2H]^{2+}$ 1186.5, showing the bY5*Y*2 ion series that corresponds to the partial sequencing of the complex tripeptide core, which in turn allowed the assignment of two disulfide pairs: Cys4 to Cys24 and Cys10 to Cys29. C, MS/MS spectrum from the precursor ion at *m/z* 972.32 that corresponds to the C-terminal end of anuroctoxin. The b8 ion at *m/z* 955.32 corresponds to the ammonia loss from the amidated Lys35 residue. All y-ion series values possess 1 atomic mass unit less than expected for the theoretical sequence inserted in the figure, and all b-ion series have the same experimental and theoretical values (except for b8), which defines the amidated C-terminal residue.

kinetics of the channel block and its removal by washout is relatively fast (Fig. 5B). A more detailed analysis of the kinetics of these processes is hindered by the minimum necessary time interval between the successive data points set by the slow recovery from inactivation of Kv1.3 channels.

Fig. 5C demonstrates that during the fully reversible block, 0.5 nM anuroctoxin did not change the current-voltage relationship of the Kv1.3 channels. The threshold for activation of the current was -42.5 ± 4.8 mV ($n = 4$) in control conditions, whereas the activation threshold was -42.5 ± 2.5 mV ($n = 4$) in the presence of 0.6 nM anuroctoxin ($p > 0.9$). The remaining fraction of the current at each test potential was calculated as I/I_0, where I is the peak current in the presence of 0.6 nM anuroctoxin and I_0 is the peak current measured in control solution. Peak currents were uniformly reduced in the presence of anuroctoxin (0.6 nM); the remaining fractions of the currents were 0.59 ± 0.07 at -20 mV, 0.51 ± 0.02 at 0 mV, 0.51 ± 0.03 at $+20$ mV, and 0.50 ± 0.03 at $+40$ mV test potentials ($n = 4$).

```
                                  10        20        30        40          %I
                         ....|....|....|....|....|....|....|....|...
1.1|ChTx(2crd)           ---ZFTNVSCTTSKECWSVCQRLHNTSRG-KCMN---KKCRCYS---- 31
2.1|Ntx (1sxm)           ---TIINVKCTSPKQCSKPCKELYGSSAGAKCMN---GKCKCYNN--- 37
3.1|Ktx (2ktx)           --GVEINVKCSGSPQCLKPCKDA-GMRFG-KCMN---RKCHCTP---- 32
4.1|TsTXKa (1hp2)        ---VFINAKCRGSPECLPKCKEAIGKAAG-KCMN---GKCKCYP---- 33
4.2|Tsk (1tsk)           ---VVIGQRCYRSPDCYSACKKLVGKATG-KCTN---GRCDC------ 26
5.1|Scytx (1scy)         --------AFCN-LRMCQLSCRS-LGLL-G-KCIG---DKCECVKH--- 28
6.1|Pi1                  -------LVKCRGTSDCGRPCQQQTGCPNS-KCIN---RMCKCYG-C-- 36
6.2|MauTx (1txm)         --------VSCTGSKDCYAPCRKQTGCPNA-KCIN---KSCKCYG-C-- 42
6.3|HsTx1 (1quz)         --------ASCRTPKDCADPCRKETGCPYG-KCMN---RKCKCNR-C-- 50
6.4|Pi4 (1n8m)           -----IEAIRCGGSRDCYRPCQKRTGCPNA-KCIN---KTCKCYG-CS- 34
6.5|Pi7 (1qky)           -----DEAIRCTGTKDCYIPCRYITGCFNS-RCIN---KSCKCYG-CT- 34
6.6|OcKTx1               -----AEVIKCRTPKDCAGPCRKQTGCPHG-KCMN---RTCRCNR-C-- 45
6.7|OcKTx2               -----AEVIKCRTPKDCADPCRKQTGCPHG-KCMN---RTCRCNR-C-- 45
6.8|OcKTx3               -----AEVIKCRTPKDCAGPCRKQTGCPHA-KCMN---KTCRCHR-C-- 39
6.9|OcKTx4               ------AIIRCSGTRECYAPCQKLTGCLNA-KCMN---KACKCYG-CV- 39
6.10|OcKTx5              -----AEVIRCSGSKQCYGPCKQQTGCTNS-KCMN-----CKCYG-C-- 37
6.11|IsTx (1wmt)         ---VHTNIPCRGTSDCYEPCEKKTNCARA-KCMN---RHCNCYNNCPW 34
6.12|Anuroctoxin         ------ZKECTGPQHCTNFCRKNK-CTHG-KCMN---RKCKCFNCK-- 100
7.1|Pi2 (2pta)           ------TISCTNPKQCYPHCKKETGYPNA-KCMN---RKCKCFGR---- 44
8.1|P01 (1acw)           --------VSC---EDCPEHCSTQKAQA---KCDN---DKCVCEPI---- 25
9.1|Bmp02 (1du9)         --------VGC---EECPMHCKGKNAKP---TCDD---GVCNCN-V---- 17
10.1|Cotx    (1pjv)      --------AVCV-YRTCDKDCKR-RGYRSG-KCIN---NACKCYPY---- 25
11.1|PBTx1               --DEEPKESCS-DEMCVIYCKG-EEYSTG-VCDG--PQKCKCSD------ 22
12.1|Btx (1c55)          WCSTCLDLACGASRECYDPCFKAFGRAHG-KCMN---NKCRCYT---- 31
13.1|Tc1 (1jlz)          --------AC---GSCRKKCK-----GSG-KCIN---GRCKCY------ 28
14.1|BmKK1               ---TPFAIKCATDADCSRKCP---GNP---SCRN---GFCACT------ 18
15.1|Aa1                 --QNETNKKCQ-GGSCASVCRRVIGVAAG-KCIN---GRCVCYP---- 30
16.1|Tamulotx            ---DLIDVKCISSQECWIACKKVTGRFEG-KCQN---RQCRCY------ 26
17.1|BmKK4 (1klh)        ------QTQCQSVRDCQQYCLT----PDR--CSY---GTCYCKTT---- 20
18.1|Tc32                ---TGPQTTCQ-AAMCEAGCKG-LGKSME-SCQG---DTCKCKA----- 21
19.1|BmBKTx (1q2k)       --------AACY-SSDCRVKCVA-MGFSSG-KCIN---SKCKCYK---- 31
Cll-dlp                  --------AC-QFWSCNSSCISR-GYRQG-YCWGIQYKYCQCQ------ 18
```

Fig. 3. Sequence alignment of anuroctoxin with other α-KTx member toxins. The amino acid sequence of anuroctoxin was compared with those of scorpion toxins from all 19 α-KTx subfamilies in the same conditions as described earlier by Rodriguez de la Vega and Possani (2004). One representative of each family is shown along with all members of the α-KTx subfamily 6. I%, the identity score of the peptide compared with anuroctoxin.

Fig. 5D demonstrates the dose-response curve of Kv1.3 inhibition by anuroctoxin in the 0.05 to 10 nM concentration range. The remaining fractions of the currents (RFs) were calculated at each concentration of anuroctoxin for $n = 3$ to 6 independent experiments. The dose-response curve was fit with a three-parameter Hill equation (see Fig. 5 legend). The resulting K_d and Hill coefficient were 0.73 nM and 0.99, respectively. The value of the Hill coefficient indicates that a single peptide interacts with the potassium channel pore, as expected from the stoichiometry of binding for several already studied K^+-channel–blocking scorpion toxins (Miller, 1995).

Selectivity of K^+ Channel Inhibition by Anuroctoxin. Anuroctoxin was tested for specificity against IKCa1, mKv1.1, mKv1.2, hKv1.2, rKv2.1, and *Drosophila melanogaster Shaker* IR channels (Fig. 6.) The potency of anuroctoxin to inhibit IKCa1 channels was assayed for channels expressed endogenously in human peripheral blood T lymphocytes. Fig. 6A shows whole-cell currents recorded using 1 μM free Ca^{2+} in the pipette-filling solution. This Ca^{2+} concentration is sufficient to activate maximally the Ca^{2+}-activated IKCa1 potassium channels (Grissmer et al., 1993). The applied voltage ramp evokes pure, non–voltage-gated IKCa1 currents below the activation threshold of the Kv1.3 channels, and change in the slope of the current can be used to characterize the current block (Grissmer et al., 1993). Figure 6A demonstrates clearly that 10 nM anuroctoxin has no blocking effect on the IKCa1 K^+ channel; the ratio of the slopes of the 10 nM anuroctoxin-treated and control curves was $1.06 \pm 0.02\%$ ($n = 5$, Fig. 6F). We used ChTx as a positive control in Fig. 6A because it inhibits both IKCa1 and Kv1.3 channels. The figure shows that 10 nM ChTx significantly reduces the slope of the K^+-current trace; the ratio of the slopes of the 10 nM ChTx-treated and control curves was 0.38 ± 0.06 ($n = 5$) in the membrane potential range, below the activation threshold of the Kv1.3 channels. The intercept

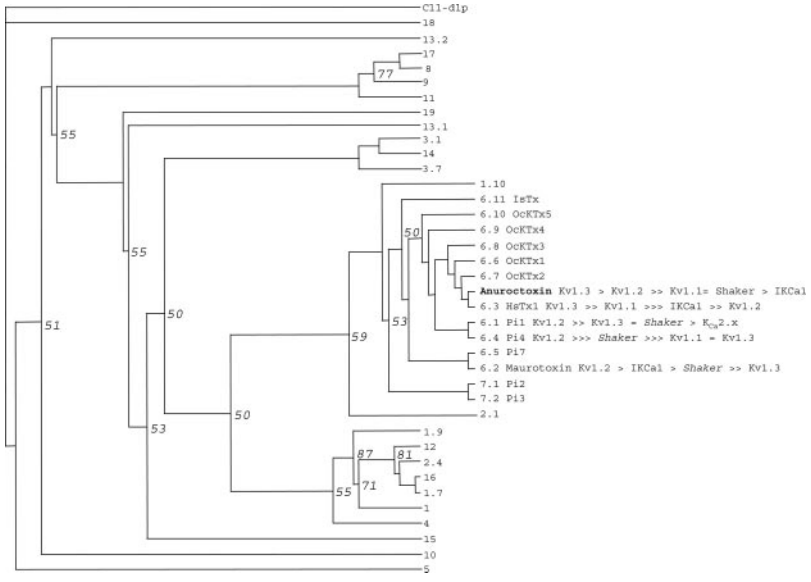

Fig. 4. Phylogenetic-based clustering of anuroctoxin. One of the 1000 sampled trees with best probability scores in the Bayesian phylogenetic reconstruction is shown. Markov chain Monte Carlo sampling with three chains (two heated) was run for 500,000 iterations. The trees were sampled every 250th generation. Convergence was attained around 200,000 generations, and the first sampled 1000 trees were discarded. For the analysis, 81 sequences of the family α-KTx were considered, plus a putative paralogous protein (Cll-dlp) used to root the tree. Groups present on the consensus tree and with a probability greater than 0.50 ($\times$100) are mapped into this tree. For clarity only, one sequence for each subfamily is shown, except for the case in which a given peptide falls outside the cluster of its assigned subfamily. All of the members of subfamilies 6 and 7 are shown. Branch tips are labeled with the systematic numbering of the subfamily. Within subfamily 6, the relative potency on various channels is indicated [data from Pi1 (Peter et al., 2000; Mouhat et al., 2004), Pi4 (M'Barek et al., 2003), MauTx (Regaya et al., 2004), and HsTx1 (Regaya et al., 2004)].

of the 10 nM ChTx-treated and control traces is between −70 and −80 mV (n = 5), and the intercept corresponds to the 0 current level (broken horizontal line). These data are consistent with the calculated reversal potential of a perfectly K^+-selective conductance (−86 mV), indicating that the dominant conductance responsible for the whole-cell currents shown in Fig. 6A is K^+-specific. The right side of Fig. 6A, in the membrane-potential range above the activation threshold of Kv1.3, shows that the Kv1.3 current is almost completely inhibited in the presence of 10 nM anuroctoxin, as expected from its subnanomolar affinity for Kv1.3. Current reduction in the presence of 10 nM ChTx at positive voltages, however, originates from the inhibition of both Kv1.3 and IKCa1 currents (K_d = ~3 nM for Kv1.3 inhibition and ~5 nM for IKCa1 inhibition) (Chandy et al., 2004).

Figure 6, B to E, show current traces obtained at +50 mV test potential in the absence and presence of 10 nM anuroctoxin for *D. melanogaster Shaker* IR channels (lacking N-type inactivation, B), rKv2.1 channels (C), mKv1.1 channels (D), and rKv1.2 channels (E) expressed in various expression

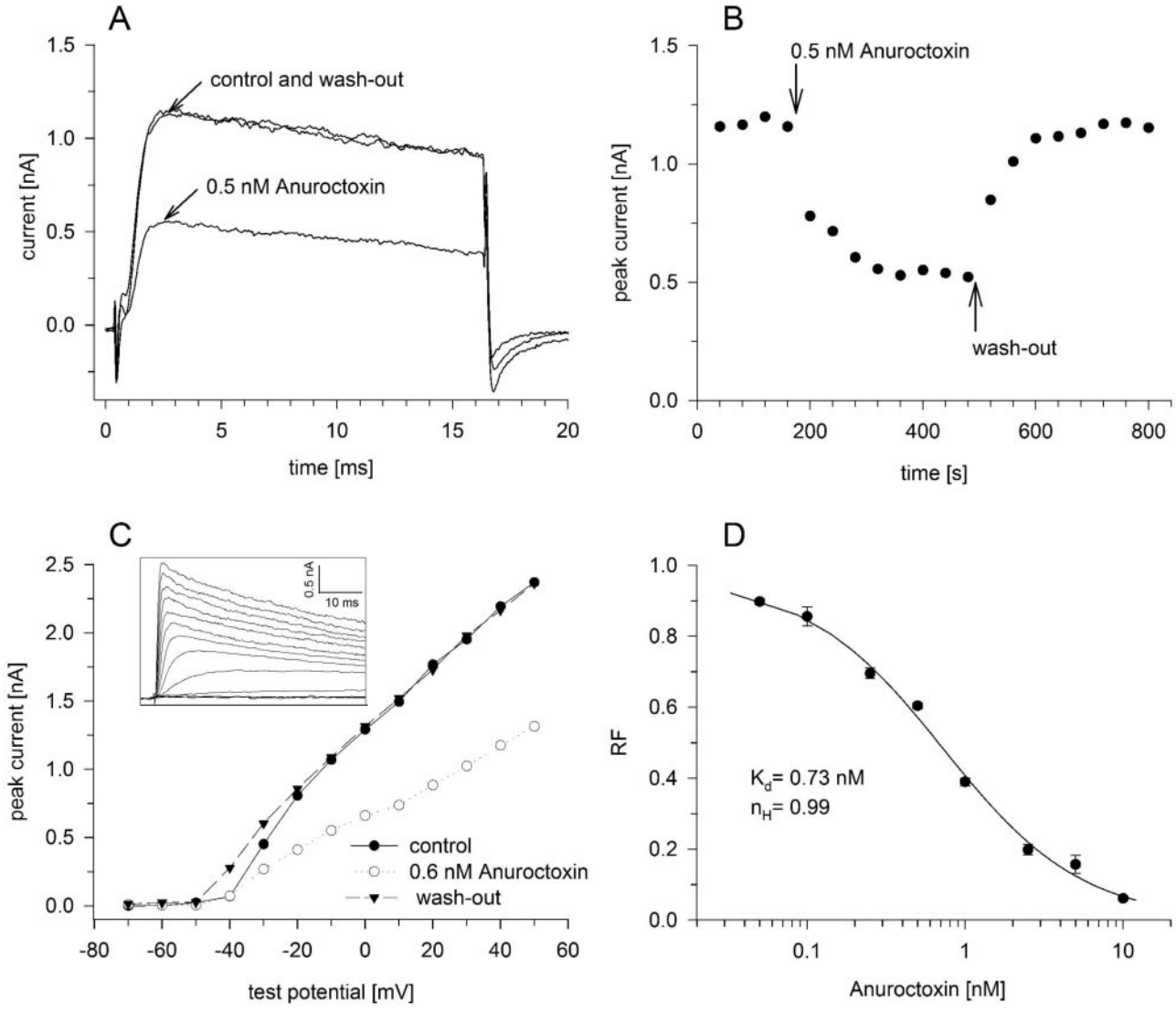

Fig. 5. Anuroctoxin reversibly blocks whole-cell Kv1.3 currents in human T lymphocytes with high affinity. A, K^+ currents of a human peripheral blood T lymphocyte were recorded in whole-cell configuration during 16-ms-long test pulses to +50 mV from a holding potential of −120 mV. Test pulses were applied every 40 s. The bath was perfused continuously. Representative traces show the K^+ current before the application of the toxin (control), after the equilibration of the block in the presence of 0.5 nM anuroctoxin (as indicated), and after the full recovery from block during the perfusion of the bath with toxin-free solution (washout). B, time courses of the development and the removal of K^+ current block. The voltage protocol and other experimental conditions were the same as in A. Peak K^+ currents were determined and plotted as a function of time. Down and up arrows indicate the start and the end of perfusion with 0.5 nM anuroctoxin, respectively. C, current-voltage relationship in the absence and presence of anuroctoxin. Inset, whole-cell K^+ currents were recorded during 200-ms-long pulses to different test potentials from a holding potential of −120 mV. Test potentials ranging from −70 to +50 mV in 10-mV increments were delivered every 40 s. The inset shows the first 50 ms of the records belonging to the control curve measured before application of anuroctoxin. Peak currents of these traces were measured and plotted as a function of the test potential (control, ●). The same protocol and analysis was repeated in the presence of 0.6 nM anuroctoxin (○) and after the washout of the toxin (▼). D, dose-response of K^+-current block by anuroctoxin. The RF was calculated as I/I_o, where I_o and I are the peak K^+ currents measured in the control solution and during bath perfusion with the test solution containing the toxin at indicated concentrations, respectively. The voltage protocol and other experimental conditions were the same as in A. The superimposed solid line is the binding curve fitted to the data points: $RF = A*K_d^{n_H}/(K_d^{n_H} + [Tx]^{n_H})$, where [Tx] indicates the toxin concentration, K_d is the dissociation constant, n_H is the Hill coefficient, and A is the saturating level of the expression in the absence of the toxin. The best fit resulted in K_d = 0.73 nM, n = 0.99, and A = 0.96. Error bars indicate S.E.M. (n = 3–6).

systems (see *Materials and Methods*). In all cases, the inhibition of the whole-cell K^+ currents by anuroctoxin was fully reversible, as indicated by the overlap of the current traces recorded before the application of the toxin and after the washout of the drug. The RF for each channel type plus for the hKv1.2 channel at 10 nM anuroctoxin concentration was determined for $n \geq 4$ independent experiments (Fig. 6F). The data indicate that the order of the blocking potency of anuroctoxin for various K^+ channels is Kv1.3 > rKv1.2 = hKv1.2 $\gg$ Shaker-IR $\approx$ mKv1.1 $\approx$ rKv2.1 > IKCa1. Thus, of the panel of channels examined, besides Kv1.3 channels, only Kv1.2 channels are inhibited significantly by 10 nM anuroctoxin. The K_d value obtained from the dose-response relationship was 5 ± 0.28 nM for the rKv1.2 channel (data not shown). Human Kv1.2 channels, which differ from the rat counterpart in one amino acid in the pore region (Glu355 in hKv1.2 corresponds to Asp355 in rKv1.2), were inhibited by 10 nM anuroctoxin essentially to the same extent as the rKv1.2. Assuming the interaction of a single peptide with an ion channel, the estimate of the K_d for hKv1.2 was calculated from the RF values obtained at a single anuroctoxin concentration as $K_d = RF \times [toxin]/(1 - RF)$. This calculation resulted in $K_d = 6.14 \pm 0.7$ nM ($n = 6$) for this channel, indicating a similar potency of anuroctoxin for the two Kv1.2 homologs.

Homology Modeling. The subfamily α-KTx 6 contains several of the most promiscuous of all K^+-channel–specific scorpion toxins in terms of their pharmacological actions (Rodriguez de la Vega and Possani, 2004), although some peptides have exquisite selectivity (see, for example, Pi4, which affects Kv1.2 with at least 1000-fold preference over other ion channels tested) (M'Barek et al., 2003). This is in contrast with other α-KTx subfamilies that show more homogeneous pharmacological properties. To address whether

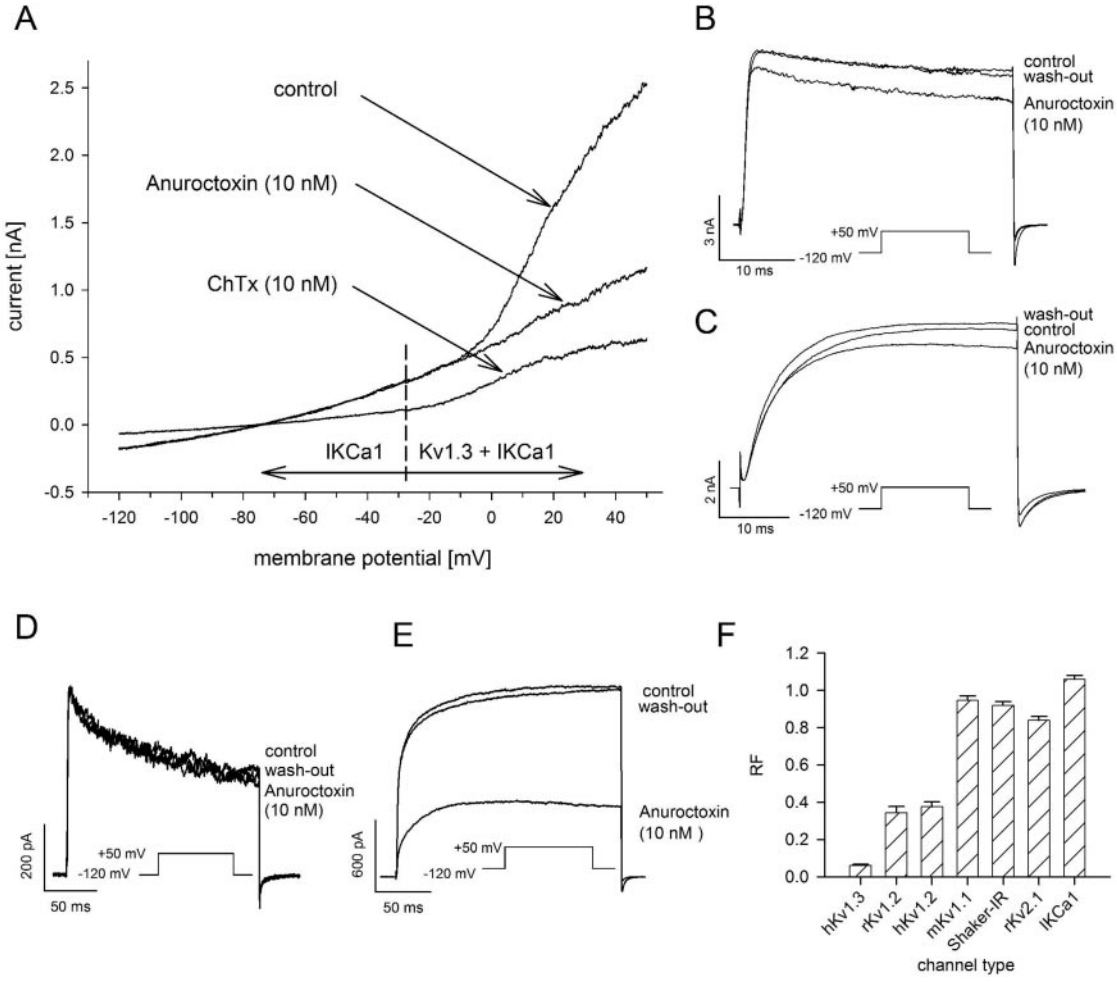

Fig. 6. Pharmacological profile of anuroctoxin. A, IKCa1 current was measured in human peripheral lymphocytes during voltage ramps from −120 to +50 mV with a rate of 1.176 mV/ms. Before the voltage ramp, the holding potential was −80 mV. Both IKCa1 and Kv1.3 channels were activated in this membrane-potential range. Pure IKCa1 current was measured below the activation threshold of Kv1.3 channels (left of the broken vertical line); on the other hand, a mixture of Kv1.3 and IKCa1 current was present above this voltage (right of the broken line). Control currents were recorded in toxin-free bath solution; ChTx and anuroctoxin were applied in the indicated concentrations. The displayed current traces in the presence of the toxins were recorded after the equilibration of the block. B to E, *Shaker* IR (B), rKv2.1 (C), mKv1.1 (D), and rKv1.2 (E) currents were evoked by voltage-clamp protocols shown in the insets before (control), during the external application of 10 nM anuroctoxin, and after its removal by washout. In all cases, sufficient time was allowed between recordings at the holding potential for the complete recovery of the channels from inactivation (interpulse intervals were 5, 30, 15, and 15 s for *Shaker* IR, Kv2.1, Kv1.1, and Kv1.2 records, respectively). F, RF was calculated as I/I_o, where I_o and I are the peak K^+ currents measured in the control solution and during bath perfusion with the test solution containing 10 nM anuroctoxin, respectively. Data are represented as mean ± S.E.M. for $n \geq 4$ independent determinations. Ion channels were expressed endogenously in human T cells (Kv1.3, IKCa1) or in various expression systems (CTLL-2 for *Shaker* IR and rKv2.1, L929 for mKv1.1, B82 for rKv1.2, and Cos-7 for hKv1.2, see *Materials and Methods* for details). Pulse protocols in B through E of this figure were the same as in Fig. 5A.

some distinctive structural features would be present in anuroctoxin that distinguish it from other α-KTx subfamily 6 members, a 3D model was obtained by homology modeling, structural minimization, and molecular dynamics (Fig. 7A). To construct the model, the amino acid sequence of anuroctoxin was aligned with those of other peptides of α-KTx subfamily 6. On the basis of this alignment, the initial 3D model was obtained in the Swiss-Modeler suite (Schwede et al., 2003), taking the structure of HsTX1 (PDB code 1quz) as the template. The model was later minimized by 3000-step gradient on NAMD and then subjected to molecular dynamics for 2 ns until the structure converged. The final model is considerably better than the initial one (dE $>$ 7056 arbitrary units) and has far fewer geometry violations, as verified by the WAT_CHECK program.

Discussion

In this article, we have described the isolation and the complete covalent structure determination of anuroctoxin. This is the first peptide isolated from *A. phaiodactylus* belonging to the Iuridae family of scorpions. When we analyzed the structure of anuroctoxin in the context of what is known for the other KTxs (Rodriguez de la Vega and Possani, 2004), it is clear that its structure is quite different. Two main points have to be considered: the peptide is blocked both at the N- and C-terminal amino acids. The first residue is pyroglutamic acid (cyclic form of glutamine), similar to what was shown to be present in charybdotoxin, and the last residue Lys35 is amidated, such as is the case of noxiustoxin (Ntx). Thus, it is a rare example in which the amino acids situated at both extremes of the peptide are blocked.

The second point is that it has a low score of similarity compared with all the other known scorpion toxins (more than 120 peptides) (Rodriguez de la Vega and Possani, 2004); identities are generally lower than 40% (Fig. 3). This, according to the systematic classification proposed by Tytgat et al. (1999), indicates that this peptide should be considered to be the first member of a new subfamily of α-KTx scorpion toxins. However, a phylogenetic clustering analysis taking into consideration all of the peptides belonging to the α-KTx family indicated that most of the trees obtained in the present sampling procedure include anuroctoxin in the α-KTx subfamily 6; therefore, α-KTx 6.12 was proposed as a systematic number for anuroctoxin. (With few exceptions, the phylogenetic analysis used here groups all members of the α-KTx subfamilies in a strongly supported monophyletic groups; 14 of the 19 subfamilies described previously are well-defined; see Supplemental Fig. S1.) Overall identities of anuroctoxin with any of the peptides included in the subfamily 6 are lower than 45%, except for HsTx1 (α-KTx 6.3), for which it is 50%. This degree of similarity is not significantly different comparing anuroctoxin with the peptides of subfamily 7 (43% for both Pi2 and Pi3). The results obtained here suggest that when a highly divergent family of proteins is analyzed, it is recommended to use a more rigorous analytic method rather than to conduct a simple similarity or identity search.

Patch-clamp experiments showed that anuroctoxin is a potent blocker of Kv1.3 channels, the dominant voltage-gated ion channels in resting and chronically activated lymphocytes of the T_{EM} phenotype (Matteson and Deutsch, 1984; Wulff et al., 2003). The block of Kv1.3 channels by anuroctoxin is very similar to the action of other scorpion toxins (Miller, 1995; Garcia et al., 2001) (Fig. 5.); the activation-gating machinery of the channels is not affected by the blocker, and the current-voltage relationship in the presence of the toxin is simply scaled-down compared with the control record. The latter argues for a voltage-independent block of the channels, which apparently contradicts the general blocking mechanism of scorpion toxins, in which a positively charged central lysine (Lys27 in ChTx), entering the pore of the channels, confers voltage-dependence to the block (Goldstein and Miller, 1993). Since the development of and recovery from anuroctoxin block of Kv1.3 channels is on the order of tens of seconds, the true voltage dependence of block cannot be determined from the measurement of peak currents during short depolarizations to different test potentials used

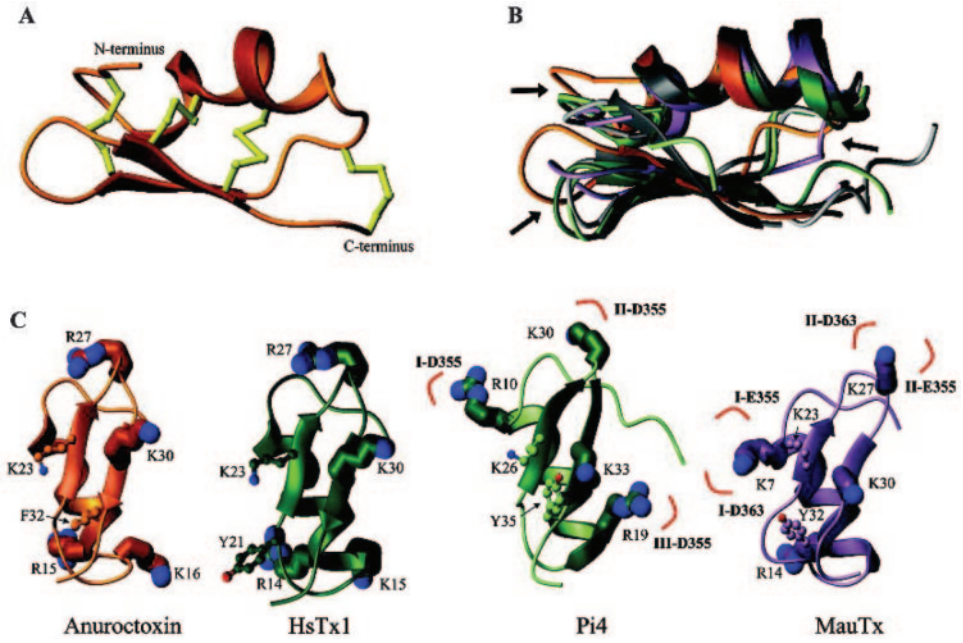

Fig. 7. Homology model of anuroctoxin and comparison with other scorpion toxins. The model of anuroctoxin (orange) calculated in Swiss-Model suite and refined with NAMD, and representative solution structures of maurotoxin (1txm, purple), HsTx1 (1quz, dark green), Pi4 (1n8m, pale green), and IsTx (1wmt, gray) are displayed with MolMol (Koradi et al., 1996). A, ribbon diagram of the final model, showing the four disulfide bridges. B, superimposition of the structures of the α-KTx subfamily members (root mean square deviation values of 1.39 Å for MauTx, 1.39 Å for HsTx1, 1.38 Å, for Pi4 and 1.38 Å for IsTx). Arrows indicate zones of high structural variability. C, "basic ring" (space-filled representation) and "functional dyad" (ball-and-chain representation) residues of HsTx1, Pi4, MauTx, and anuroctoxin in the same orientation. Note the differences in spatial localization of the basic ring residues. The putative contact amino acids on the respective channels [Pi4 with rKv1.2 (M'Barek et al., 2003) and MauTx with human Kv1.2 (Visan et al., 2004)] are indicated.

in this study, as discussed in detail elsewhere (Peter et al., 2001). The block of Kv1.3 currents is fully reversible, and the dose-response curve of anuroctoxin for Kv1.3 inhibition is characterized by a Hill coefficient ~1, suggesting that a single peptide interacts with the channel, similarly to other scorpion toxins.

The sequence alignment (Fig. 3) shows that K23 in anuroctoxin corresponds to K27 in ChTx, and an aromatic residue in anuroctoxin (Phe32) corresponds to Tyr36 in ChTx. Thus, the essential dyad of critically positioned amino acids required for K^+-channel recognition is also found in the sequence of anuroctoxin (Dauplais et al., 1997). To determine whether the steric requirements for the formation of the essential dyad are valid for anuroctoxin, its putative three-dimensional structure was generated by template modeling using the coordinates known from the structure of HsTx1 (PDB code 1quz). This scorpion toxin was used as a template because it belongs to the same subfamily as anuroctoxin with the highest overall identity score (50%), and it also has four disulfide bridges and displays high affinity for Kv1.3 (Lebrun et al., 1997). The model indicates that the overall structure of anuroctoxin is similar to that of ChTx, although Phe32 is positioned more than 7 Å apart from the α carbon of Lys23, a critical distance that was considered to be a hallmark for the activity of other peptide toxins (Dauplais et al., 1997).

These arguments suggest that anuroctoxin acts as a classic pore blocker of Kv1.3 channels, similarly to other scorpion toxins. Further experiments are needed to identify the unique interaction partners between anuroctoxin and the toxin receptor site in Kv1.3, which govern high-affinity binding.

Regarding T-cell physiology, the most important factor in the pharmacological profile of anuroctoxin is its selectivity for Kv1.3 over IKCa1, the Ca^+-activated K^+ channel of human T lymphocytes. Although the limited amount of the toxin prevented the determination of a dose-response curve for the interaction with IKCa1, a lack of block at 10 nM anuroctoxin concentration allows the lowest estimate of ~1000 times selectivity ratio for Kv1.3 over IKCa1.

Several high-affinity peptide blockers of Kv1.3 are selective for Kv1.3 over IKCa1, similarly to anuroctoxin. These include scorpion toxins (e.g., MgTx, Ntx, and kaliotoxin) and ShK toxin isolated from sea anemone. However, ion channels important in neuronal and muscle excitability are also inhibited by these toxins with nanomolar-picomolar affinities [e.g., Kv1.1 by ShK (Kalman et al., 1998) and kaliotoxin (Grissmer et al., 1994), whereas Kv1.2 is inhibited by MgTx (Koch et al., 1997) and Ntx (Grissmer et al., 1994)]. Of the panel of channels studied (Shaker, Kv1.1, Kv1.2, and Kv2.1), anuroctoxin inhibited only Kv1.2 channels significantly with approximately 7-fold lower affinity than Kv1.3 channels. Within subfamily 6 of α-KTx, the only high-affinity blocker of Kv1.3 is HsTx1, which also inhibits Kv1.1 channels with nanomolar affinity (K_d = 7 nM) and IKCa1 channels with a modest/low affinity (K_d = 460 nM) (Regaya et al., 2004). Thus, although phylogenetic analysis classifies anuroctoxin into subfamily 6, its pharmacological profile is similar to that of MgTx (α-KTx 2.2) and Ntx (α-KTx 2.1).

All of the α-KTx peptides have very similar cysteine stabilized-α/β core. In particular, the members of the subfamily 6 have root mean square deviation values of 1.5 Å for elements of the secondary structure (Fig. 7B). However, it is worth noting that the regions surrounding the common pore-blocker pharmacophore have very divergent conformations (Fig. 7B). It is interesting that three of four positions of Pi4 proposed to be involved in Kv1.2 specificity (basic ring residues) occupy these regions (M'Barek et al., 2003). Likewise, two positions of maurotoxin (MauTx) critical for the recognition of human Kv1.2, identified by double-mutant cycle (Visan et al., 2004), occupied exactly the same positions. All peptides for which the 3D structure is known have a basic ring surrounding the equatorial position of the structure, apart from the site of the "functional dyad", which fits more closely to the mouth of the ion channels (see diagram in Fig. 7C). Thus, it is tempting to speculate that the interaction of different basic residues situated in this ring of the various toxins may affect in a differential manner distinct subtypes of K^+ channels that are recognized by these toxins, as already suggested for Pi4 (M'Barek et al., 2003), Pi1 (Mouhat et al., 2004), and MauTx (Visan et al., 2004). The two toxins from subfamily α-KTx 6 that have high affinity for Kv1.3 (anuroctoxin and HsTx1) share a similar distribution of positively charged residues. These toxins are different from those that have high affinity for other Kv channels (e.g., MauTx and Pi4).

The selectivity of anuroctoxin for Kv1.3 over IKCa1 confers an important pharmacological potency to this toxin for the regulation of T-cell activation. This derives from the recent discovery of human T-cell subtype-specific expression of Kv1.3 and IKCa1 channels upon activation and the ability of suppressing the proliferation of $Kv1.3^{high}IKCa1^{low}$ T_{EM} cells specifically by selective Kv1.3 inhibitors. Thus, a Kv1.3-based therapy that suppresses the activation of T_{EM} cells without significant impairment of the proliferation of naive and T_{CM} cells may establish a therapeutic potential for multiple sclerosis and other T-cell–mediated immune diseases, such as type I diabetes mellitus, inflammatory bone resorption in experimental periodontal disease (Valverde et al., 2004), and chronic graft rejection and graft-versus-host disease sustained probably by chronically activated T_{EM} cells (Yamashita et al., 2004).

In summary, we have isolated, purified, and electrophysiologically characterized a new α-KTx toxin, anuroctoxin (α-KTx 6.12). The unique primary structure of the toxin, along with its selectivity for Kv1.3 over IKCa1, makes this toxin pharmacologically interesting and valuable.

Acknowledgments

Helpful discussions with Laura Dominguez on the modeling procedures and the assistance of Saida Patricia Salas-Castillo during HPLC separation are greatly acknowledged.

References

Batista CV, del Pozo L, Zamudio FZ, Contreras S, Becerril B, Wanke E, and Possani LD (2004) Proteomics of the venom from the Amazonian scorpion *Tityus cambridgei* and the role of prolines on mass spectrometry analysis of toxins. *J Chromatogr B Analyt Technol Biomed Life Sci* **803:**55–66.

Cahalan MD, Wulff H, and Chandy KG (2001) Molecular properties and physiological roles of ion channels in the immune system. *J Clin Immunol* **21:**235–252.

Chandy KG, Wulff H, Beeton C, Pennington M, Gutman GA, and Cahalan MD (2004) K^+ channels as targets for specific immunomodulation. *Trends Pharmacol Sci* **25:**280–289.

Dauplais M, Lecoq A, Song J, Cotton J, Jamin N, Gilquin B, Roumestand C, Vita C, de Medeiros CL, Rowan EG, et al. (1997) On the convergent evolution of animal toxins. Conservation of a diad of functional residues in potassium channel-blocking toxins with unrelated structures. *J Biol Chem* **272:**4302–4309.

Deutsch C and Chen L-Q (1993) Heterologous expression of specific K^+ channels in T lymphocytes: functional consequences for volume regulation. *Proc Natl Acad Sci USA* **90:**10036–10040.

Deutsch C, Krause D, and Lee SC (1986) Voltage-gated potassium conductance in human T lymphocytes stimulated with phorbol ester. *J Physiol (Lond)* **372:**405–423.

Edgar RC (2004) MUSCLE: multiple sequence alignment with high accuracy and high throughput. *Nucleic Acids Res* **32:**1792–1797.

Garcia ML, Gao Y, McManus OB, and Kaczorowski GJ (2001) Potassium channels: from scorpion venoms to high-resolution structure. *Toxicon* **39:**739–748.

Goldstein SA and Miller C (1993) Mechanism of charybdotoxin block of a voltage-gated K^+ channel. *Biophys J* **65:**1613–1619.

Grissmer S, Nguyen AN, Aiyar J, Hanson DC, Mather RJ, Gutman GA, Karmilowicz MJ, Auperin DD, and Chandy KG (1994) Pharmacological characterization of five cloned voltage-gated K^+ channels, types Kv1.1, 1.2, 1.3, 1.5 and 3.1, stably expressed in mammalian cell lines. *Mol Pharmacol* **45:**1227–1234.

Grissmer S, Nguyen AN, and Cahalan MD (1993) Calcium-activated potassium channels in resting and activated human T lymphocytes. Expression levels, calcium dependence, ion selectivity and pharmacology. *J Gen Physiol* **102:**601–630.

Jiang Y, Lee A, Chen J, Ruta V, Cadene M, Chait BT, and MacKinnon R (2003) X-ray structure of a voltage-dependent K+ channel. *Nature (Lond)* **423:**33–41.

Jones DT, Taylor WR, and Thornton JM (1992) The rapid generation of mutation data matrices from protein sequences. *Comput Appl Biosci* **8:**275–282.

Kale L, Skeel R, Bhandarkar M, Brunner R, Gursoy A, Krawetz N, Phillips J, Shinozaki A, Varadarjan K, and Schulten K (1999) NAMD2: greater scalability for parallel molecular dynamics. *J Comp Phys* **151:**283–312.

Kalman K, Pennington MW, Lanigan MD, Nguyen A, Rauer H, Mahnir V, Paschetto K, Kem WR, Grissmer S, Gutman GA, et al. (1998) ShK-Dap22, a potent Kv1.3-specific immunosuppressive polypeptide. *J Biol Chem* **273:**32697–32707.

Koch RO, Wanner SG, Koschak A, Hanner M, Schwarzer C, Kaczorowski GJ, Slaughter RS, Garcia ML, and Knaus HG (1997) Complex subunit assembly of neuronal voltage-gated K+ channels. Basis for high-affinity toxin interactions and pharmacology. *J Biol Chem* **272:**27577–27581.

Koradi R, Billeter M, and Wuthrich K (1996) MOLMOL: a program for display and analysis of macromolecular structures. *J Mol Graph* **14:**29–32.

Lebrun B, Romi-Lebrun R, Martin-Eauclaire MF, Yasuda A, Ishiguro M, Oyama Y, Pongs O, and Nakajima T (1997) A four-disulphide-bridged toxin, with high affinity towards voltage-gated K+ channels, isolated from heterometrus spinnifer (*Scorpionidae*) venom. *Biochem J* **328:**321–327.

Leonard RJ, Garcia ML, Slaughter RS, and Reuben JP (1992) Selective blockers of voltage-gated K+ channels depolarize human T lymphocytes: mechanism of the antiproliferative effect of charybdotoxin. *Proc Natl Acad Sci USA* **89:**10094–10098.

Matteson DR and Deutsch C (1984) K channels in T lymphocytes: a patch clamp study using monoclonal antibody adhesion. *Nature (Lond)* **307:**468–471.

M'Barek S, Mosbah A, Sandoz G, Fajloun Z, Olamendi-Portugal T, Rochat H, Sampieri F, Guijarro JI, Mansuelle P, Delepierre M, et al. (2003) Synthesis and characterization of Pi4, a scorpion toxin from pandinus imperator that acts on K+ channels. *Eur J Biochem* **270:**3583–3592.

Miller C (1995) The charybdotoxin family of K^+-channel-blocking peptides. *Neuron* **15:**5–10.

Mouhat S, Mosbah A, Visan V, Wulff H, Delepierre M, Darbon H, Grissmer S, De Waard M, and Sabatier JM (2004) The "functional" dyad of scorpion toxin Pi1 is not itself a prerequisite for toxin binding to the voltage-gated Kv1.2 potassium channels. *Biochem J* **377:**25–36.

Panyi G, Varga Z, and Gaspar R (2004) Ion channels and lymphocyte activation. *Immunol Lett* **92:**55–66.

Pardo-Lopez L, Zhang M, Liu J, Jiang M, Possani LD, and Tseng GN (2002) Mapping the binding site of a human ether-a-go-go-related gene-specific peptide toxin (ErgTx) to the channel's outer vestibule. *J Biol Chem* **277:**16403–16411.

Peter M, Hajdu P, Varga Z, Damjanovich S, Possani LD, Panyi G, and Gaspar R (2000) Blockage of human T lymphocyte Kv1.3 channels by Pi1, a novel class of scorpion toxin. *Biochem Biophys Res Commun* **278:**34–37.

Peter MJ, Varga Z, Hajdu P, Gaspar RJ, Damjanovich S, Horjales E, Possani LD, and Panyi G (2001) Effects of toxins Pi2 and Pi3 on human T lymphocyte Kv1.3 channels: the role of Glu7 and Lys24. *J Membr Biol* **179:**13–25.

Regaya I, Beeton C, Ferrat G, Andreotti N, Darbon H, De Waard M, and Sabatier JM (2004) Evidence for domain-specific recognition of SK and Kv channels by MTX and HsTx1 scorpion toxins. *J Biol Chem* **279:**55690–55696.

Rodriguez de la Vega RC, Garcia BI, D'Ambrosio C, Diego-Garcia E, Scaloni A, and Possani LD (2004) Antimicrobial peptide induction in the haemolymph of the Mexican scorpion Centruroides limpidus limpidus in response to septic injury. *Cell Mol Life Sci* **61:**1507–1519.

Ronquist F and Huelsenbeck JP (2003) MrBayes 3: Bayesian phylogenetic inference under mixed models. *Bioinformatics* **19:**1572–1574.

Sallusto F, Geginat J, and Lanzavecchia A (2004) Central memory and effector memory T cell subsets: function, generation and maintenance. *Annu Rev Immunol* **22:**745–763.

Schwede T, Kopp J, Guex N, and Peitsch MC (2003) SWISS-MODEL: an automated protein homology-modeling server. *Nucleic Acids Res* **31:**3381–3385.

Tytgat J, Chandy KG, Garcia ML, Gutman GA, Martin-Eauclaire MF, van der Walt JJ, and Possani LD (1999) A unified nomenclature for short-chain peptides isolated from scorpion venoms: alpha-KTx molecular subfamilies. *Trends Pharmacol Sci* **20:**444–447.

Valdez-Cruz NA, Batista CV, and Possani LD (2004) Phaiodactylipin, a glycosylated heterodimeric phospholipase A from the venom of the scorpion *Anuroctonus phaiodactylus*. *Eur J Biochem* **271:**1453–1464.

Valverde P, Kawai T, and Taubman MA (2004) Selective blockade of voltage-gated potassium channels reduces inflammatory bone resorption in experimental periodontal disease. *J Bone Miner Res* **19:**155–164.

Visan V, Fajloun Z, Sabatier JM, and Grissmer S (2004) Mapping of maurotoxin binding sites on HKv1.2, HKv1.3, and HIKCa1 channels. *Mol Pharmacol* **66:**1103–1112.

Wulff H, Calabresi PA, Allie R, Yun S, Pennington M, Beeton C, and Chandy KG (2003) The voltage-gated Kv1.3 K^+ channel in effector memory T cells as new target for MS. *J Clin Investig* **111:**1703–1713.

Xu CQ, Brone B, Wicher D, Bozkurt O, Lu WY, Huys I, Han YH, Tytgat J, Van Kerkhove E, and Chi CW (2004) BmBKTx1, a novel Ca2+-activated K+ channel blocker purified from the Asian scorpion *Buthus martensi* Karsch. *J Biol Chem* **279:**34562–34569.

Yamashita K, Choi U, Woltz PC, Foster S, Sneller MC, Hakim FT, and Fowler DH (2004) Severe chronic graft-versus-host disease is characterized by a preponderance of $CD4^+$ effector memory cells relative to central memory cells. *Blood* **103:**3986–3988.

Address correspondence to: Dr. György Panyi, Department of Biophysics and Cell Biology, University of Debrecen, Medical and Health Science Center, 98 Nagyerdei krt., Debrecen, Hungary 4012. E-mail: panyi@jaguar.dote.hu